Inorg. Chem. **2008**, *47*, 2223−2232

Cu^{I} Complexes with *N,N′,S,S′* Scorpionate Ligands: Evidence for Dimer−Monomer Equilibria

Marcello Gennari, **Matteo Tegoni**, **Maurizio Lanfranchi**, **Maria Angela Pellinghelli**, **Marco Giannetto**, **and Luciano Marchiò***

Dipartimento di Chimica Generale ed Inorganica, Chimica Analitica, Chimica Fisica, Università degli Studi di Parma, viale G. P. Usberti 17/a, I 43100 Parma, Italy

Received October 25, 2007

The heteroscorpionate *N,N′,S,S′* donor ligands 4-methoxy-3,5-dimethyl-2-(3-(methylthio)-1-(3-(2-(methylthio)phenyl)-1*H*-pyrazol-1-yl)propyl)pyridine (L^a) and 4-methoxy-3,5-dimethyl-2-(2-(methylthio)-1-(3-(2-(methylthio)phenyl)-1*H*-pyrazol-1-yl)ethyl)pyridine (L^b) were prepared. The Cu^{I} complexes $[Cu(L^a)]_2(BF_4)_2$ ($\mathbf{a_2}(BF_4)_2$) and $[Cu(L^b)]_2(BF_4)_2$ ($\mathbf{b_2}(BF_4)_2$) were synthesized and characterized by X-ray crystallography. Both compounds exhibit a dinuclear structure, presenting each Cu^{I} center in a distorted *N,N′,S,S′* tetrahedral environment. On the basis of nuclear magnetic resonance (NMR) and ESI−mass data, the presence of a mononuclear complex in equilibrium with the dimer was hypothesized for both complexes. The dimerization constants of the processes, $2\mathbf{a}^+ = \mathbf{a_2}^{2+}$ and $2\mathbf{b}^+ = \mathbf{b_2}^{2+}$, were obtained by ^{1}H NMR dilution experiments (fast-exchange regime) in CD_3CN: log $K(\mathbf{a_2}^{2+}) = 3.55(6)$ and log $K(\mathbf{b_2}^{2+}) = 3.23(5)$ at 300 K. Thermodynamic parameters were determined by a van't Hoff analysis (280−310 K temperature range): $\Delta H^0(\mathbf{a_2}^{2+}) = -12(1)$ kJ mol^{-1}, $\Delta H^0(\mathbf{b_2}^{2+}) = -10(1)$ kJ mol^{-1}, $\Delta S^0(\mathbf{a_2}^{2+}) = +27(4)$ kJ mol^{-1}, and $\Delta S^0(\mathbf{b_2}^{2+}) = +28(4)$ kJ mol^{-1}. Pulsed gradient spin–echo (PGSE) NMR experiments provided the weighted-average hydrodynamic volume (V_H) of the species present in CD_3CN solution at different copper concentrations (C_{Cu}). Nonlinear interpolation of V_H as a function of C_{Cu} for a dimer−monomer equilibrium led to the hydrodynamic volumes of both monomers (V_H^0(M)) and dimers (V_H^0(D)): $V_H^0(\mathbf{a}^+) = 620(40)$ Å^3, $V_H^0(\mathbf{b}^+) = 550(10)$ Å^3, $V_H^0(\mathbf{a_2}^{2+}) = 950(20)$ Å^3, and $V_H^0(\mathbf{b_2}^{2+}) = 900(10)$ Å^3. Cyclic voltammetry experiments performed in CH_3CN and CH_2Cl_2 showed a quasi-reversible to irreversible behavior of the Cu^{I}/Cu^{II} redox couple for both complexes.

Introduction

We are currently exploring the coordination properties of N_xS_y polydentate ligands derived from the pyrazole−pyridine moiety.[1,2] Because of the spatial arrangement of donor atoms, these ligands can be considered as part of the scorpionates ligand family,[3] and in particular, on the basis of the nonequivalence of the donor groups that surround the central atom, these compounds can be classified as heteroscorpionates.[4]

In this work, we present the coordination properties, of two C-centered tetradentate *N,N′,S,S′* donor ligands (L^a and L^b in Scheme 1) with Cu^{I}. L^a and L^b are based on an *N,N′,S*-donor-substituted pyrazole−pyridine platform, with an alkylthioether group as the fourth coordination site. The underlying idea is to design geometrically preorganized ligands with a suitable donor set that satisfies the electronic and steric

* To whom correspondence should be addressed. E-mail: marchio@unipr.it.

(1) Gennari, M.; Lanfranchi, M.; Cammi, R.; Pellinghelli, M. A.; Marchio, L. *Inorg. Chem.* **2007**, *46*, 10143–10152.

(2) Gennari, M.; Tegoni, M.; Lanfranchi, M.; Pellinghelli, M. A.; Marchio, L. *Inorg. Chem.* **2007**, *46*, 3367–3377.

(3) Trofimenko, S. *Scorpionates—The Coordination Chemistry of Polypyrazolylborate Ligands*; Imperial College Press: London, U.K., 1999.

(4) For reviews covering the coordination properties of the B-centered scorpionate ligands, see (a) Trofimenko, S. *Chem. Rev.* **1993**, *93*, 943–980. (b) Pettinari, C.; Santini, C. *Compr. Coord. Chem. II* **2004**, *1*, 159–210. For references describing the C-centered scorpionate ligands, see (c) Otero, A.; Fernandez-Baeza, J.; Antinolo, A.; Tejeda, J.; Lara-Sanchez, A. *Dalton Trans.* **2004**, *1499*, 1510. (d) Pettinari, C.; Pettinari, R. *Coord. Chem. Rev.* **2005**, *249*, 663–691. (e) Pettinari, C.; Pettinari, R. *Coord. Chem. Rev.* **2005**, *249*, 525–543. (f) Reger, D. L. *Comm. Inorg. Chem.* **1999**, *21*, 1–28. For references covering the bioinorganic applications of the scorpionate ligands, see (g) Kitajima, N.; Tolman, W. B. *Prog. Inorg. Chem.* **1995**, *43*, 419–531. (h) Parkin, G. *Chem. Commun.* **2000**, *1971*, 1985. (i) Vahrenkamp, H. *Acc. Chem. Res.* **1999**, *32*, 589–596. (l) Vahrenkamp, H. *Dalton Trans.* **2007**, *475*, 1–4759. For references releated to the catalytic applications of scorpionate ligands, see (m) Slugovc, C.; Schmid, R.; Kirchner, K. *Coord. Chem. Rev.* **1999**, *186*, 109–126. (n) Slugovc, C.; Padilla-Martinez, I.; Sirol, S.; Carmona, E. *Coord. Chem. Rev.* **2001**, *213*, 129–157. (o) Hikichi, S.; Akita, M.; Moro-Oka, Y. *Coord. Chem. Rev.* **2000**, *198*, 61–87.

10.1021/ic702108x CCC: $40.75
Published on Web 02/12/2008

Scheme 1

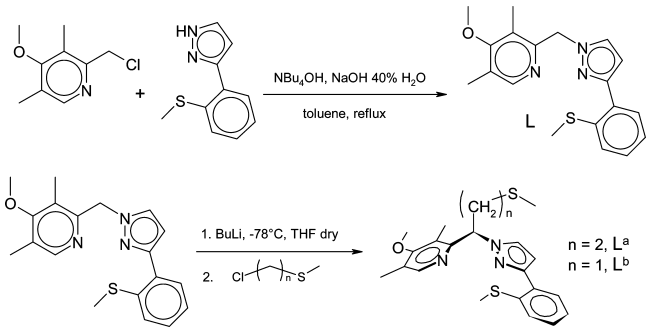

requirements of Cu^{I}, to yield mononuclear complexes exhibiting a tetrahedral geometry of the metal center. The reason for this resides in the possible exploitation of low-molecular-weight complexes as functional models of type-1 cupredoxins (electron-transfer copper proteins).[5–12] Some of these models have recently been studied as electron-transfer mediators[13] in dye-sensitized solar cells.[14]

Unfortunately, the major drawback with respect to the control of the nuclearity of the complexes presented in this work is related to the flexible nature of the alkyl-thioether moiety of the ligands, which leads to the isolation of dinuclear species at the solid state, with the thioether-sulfur bridging a second metal center, $[Cu(L^a)]_2(BF_4)_2$ ($\mathbf{a_2}(BF_4)_2$) and $[Cu(L^b)]_2(BF_4)_2$ ($\mathbf{b_2}(BF_4)_2$). It is worth noting that this molecular arrangement is also retained when diminishing the length of the thioether group from $-CH_2-CH_2SCH_3$ in L^a to $-CH_2-SCH_3$ in L^b. However, from dilution ^1H nuclear magnetic resonance (NMR) titrations and pulsed gradient spin–echo (PGSE) NMR experiments performed in CD_3CN, we found evidence of the equilibrium involving the $\mathbf{a_2}^{2+}$ and $\mathbf{b_2}^{2+}$ dimers and the corresponding mononuclear entities, $[Cu(L^a)]^+$ ($\mathbf{a}^+$) and $[Cu(L^b)]^+$ ($\mathbf{b}^+$): $\mathbf{a_2}^{2+} = \mathbf{2a}^+$ and $\mathbf{b_2}^{2+} = \mathbf{2b}^+$. Electrospray ionization−mass spectrometry (ESI−MS) in CH_3CN would confirm this hypothesis.

From a functional point of view, the electrochemical properties of the complexes were investigated by cyclic voltammetry in CH_3CN (wherein the dimerization constants were also determined) and CH_2Cl_2. A quasi-reversible to irreversible behavior of the Cu^{I}/Cu^{II} redox couple was found in all of the experimental conditions (e.g., solvent and concentration), attesting to a sizable reorganization energy during the heterogeneous electron transfer.

Experimental Section

General Procedures. All reagents and solvents were commercially available, except for 4-methoxy-3,5-dimethyl-2-((3-(2-(methylthio)phenyl)-1*H*-pyrazol-1-yl)methyl)pyridine (L)[1] and $[Cu(CH_3CN)_4]BF_4$,[15] which were prepared as previously reported. Tetrahydrofuran (THF) and dichloromethane were distilled over Na/benzophenone and CaH_2, respectively. All syntheses were performed in inert gas (N_2) using Schlenk techniques.

^1H and ^{13}C NMR spectra were recorded on a Bruker Avance 300 spectrometer using standard Bruker pulse sequences. Chemical shifts are reported in parts per million (ppm) referenced to residual solvent protons ($CDCl_3$ and CD_3CN). Mass spectra were obtained with a Micromass ZMD spectrometer. The mixtures were analyzed in positive-ionization mode by direct perfusion in the ESI−MS interface. Infrared spectra were recorded from 4000 to 700 cm^{-1} on a Perkin-Elmer FTIR Nexus spectrometer equipped with a Thermo-Nicolet microscope. Elemental analyses (C, H, and N) were performed with a Carlo Erba EA 1108 automated analyzer.

Synthesis of 4-Methoxy-3,5-dimethyl-2-(3-(methylthio)-1-(3-(2-(methylthio)phenyl)-1*H*-pyrazol-1-yl)propyl)pyridine (L^a)[16]. A solution of 4-methoxy-3,5-dimethyl-2-((3-(2-(methylthio)phenyl)-1*H*-pyrazol-1-yl)methyl)pyridine (2.15 g, 6.33 mmol) in THF (80 mL) was cooled to −78 °C, and then *n*-BuLi (4.15 mL, 1.6 M in hexane, 6.64 mmol) was slowly added. After stirring the red solution at −78 °C for 45 min, 97% 2-chloroethyl methyl sulfide (0.68 mL, $d = 1.11$ g/mL, 6.62 mmol) was added and the resulting solution was allowed to warm to room temperature with stirring. After 1 h, the clear yellow solution was dried under a vacuum and the residual solid was extracted in diethyl ether/water (80/30 mL). The organic phase was washed with brine and dried with Na_2SO_4. The solvents were removed under vacuum, giving a yellow oil that was purified by silica column chromatography (75:25 hexane/ethyl acetate), yielding a colorless oil (L^a, 1.53 g, 3.70 mmol, 58%). IR (cm^{-1}): 3054w, 2917s, 2852w, 1587m, 1563s, 1472s, 1451s, 1436s, 1395s, 1337m, 1260s, 1048s, 999s, 754vs. ^1H NMR (300 MHz, $CDCl_3$) δ: 2.11 (s, 3H, C H_3SR), 2.26 (s, 3H, C H_3 py *o*-CH), 2.35 (s, 3H, C H_3 py *p*-CH), 2.42 (s, 3H, C H_3SAr), 2.44–2.60 (m, 2H, C H_2(SCH_3)), 2.65–2.72 (m, 2H, C H_2(CH*)), 3.74 (s, 3H, C H_3O), 6.00 (m, 1H, C *H**), 6.57 (d, $J = 2.1$ Hz, 1H, C *H* pz(ph)), 7.17 (dt, 1H, $J = 7.0$, 2.0 Hz, C *H* ph), 7.28 (m, 2H, C *H* ph), 7.55 (m, 2H, C *H* pz(CH*) + C *H* ph), 8.30 (s, 1H, C *H* py). ^{13}C NMR (75 MHz, $CDCl_3$) δ: 10.6 (*C*H_3 py *p*-CH), 13.2 (*C*H_3 py *o*-CH), 15.3 (*C*H_3SR), 15.4 (*C*H_3SAr), 30.7 (*C*H_2(SCH_3)), 33.8 (*C*H_2(CH*)), 59.9 (*C*H_3O), 61.8 (*C*H*), 106.5 (*C*H pz(ph)), 124.4 (*C*H ph), 125.3 (*C*H ph), 127.7 (*C*H ph), 127.9 (*C*H ph), 129.6 (*C*H pz(CH*)), 149.1 (*C*H py). ESI−MS (p.i., 50 V, CH_3OH, *m/z*, I%): 414.6, 100, $[L^aH]^+$. Anal. Calcd for $C_{22}H_{27}N_3OS_2$ (413.60): C, 63.89; H, 6.58; N, 10.16. Found: C, 63.73; H, 6.85; N, 10.29.

Synthesis of 4-Methoxy-3,5-dimethyl-2-(2-(methylthio)-1-(3-(2-(methylthio)phenyl)-1*H*-pyrazol-1-yl)ethyl)pyridine (L^b). The same procedure used to prepare L^a was applied by using the same quantities of reagents/solvent and 95% chloromethyl methyl sulfide (0.58 mL, $d = 1.17$ g/mL, 6.67 mmol) instead of 2-chloroethyl methyl sulfide. A colorless oil was obtained (L^b, 1.52 g, 3.80 mmol, 60%). IR (cm^{-1}): 2918m, 2850w, 1587w, 1563m, 1471s, 1454s,

(5) Chaka, G.; Kandegedara, A.; Heeg, M. J.; Rorabacher, D. B. *Dalton Trans.* **2007**, *449*, 458.
(6) Corfield, P. W. R.; Ceccarelli, C.; Glick, M. D.; Moy, I. W. Y.; Ochrymowycz, L. A.; Rorabacher, D. B. *J. Am. Chem. Soc.* **1985**, *107*, 2399–2404.
(7) Gorelsky, S. I.; Basumallick, L.; Vura-Weis, J.; Sarangi, R.; Hodgson, K. O.; Hedman, B.; Fujisawa, K.; Solomon, E. I. *Inorg. Chem.* **2005**, *44*, 4947–4960.
(8) Holland, P. L.; Tolman, W. B. *J. Am. Chem. Soc.* **1999**, *121*, 7270–7271.
(9) Kitajima, N.; Fujisawa, K.; Tanaka, M.; Morooka, Y. *J. Am. Chem. Soc.* **1992**, *114*, 9232–9233.
(10) Matsunaga, Y.; Fujisawa, K.; Ibi, N.; Miyashita, Y.; Okamoto, K. *Inorg. Chem.* **2005**, *44*, 325–335.
(11) Randall, D. W.; George, S. D.; Holland, P. L.; Hedman, B.; Hodgson, K. O.; Tolman, W. B.; Solomon, E. I. *J. Am. Chem. Soc.* **2000**, *122*, 11632–11648.
(12) Vande Linde, A. M. Q.; Westerby, B. C.; Ochrymowycz, L. A.; Rorabacher, D. B. *Inorg. Chem.* **1993**, *32*, 251–257.
(13) Hattori, S.; Wada, Y.; Yanagida, S.; Fukuzumi, S. *J. Am. Chem. Soc.* **2005**, *127*, 9648–9654.
(14) Gratzel, M. *Inorg. Chem.* **2005**, *44*, 6841–6851.
(15) Leftin, J. H. *Chem. Abstr.* **1967**, *66*, 46487e.
(16) pz = pyrazole, py = pyridine, ph = phenyle, asterisk (*) = stereogenic carbon.

1432s, 1395m, 1257m br, 1211m, 1036w, 999w, 750m. ^{1}H NMR (300 MHz, $CDCl_3$) δ: 2.02 (s, 3H, CH_3SR), 2.25 (s, 3H, C H_3 py *o*-CH), 2.30 (s, 3H, C H_3 py *p*-CH), 2.38 (s, 3H, C H_3SAr), 3.33 (dd, J = 13.3, 5.9 Hz, 1H, *H*CH(CH*)), 3.65 (dd, J = 13.3, 8.9 Hz, 1H, *H*′CH(CH*)), 3.72 (s, 3H, C H_3O), 5.95 (dd, J = 8.8, 6.0 Hz, 1H, C *H**), 6.53 (d, J = 2.4 Hz, 1H, C *H* pz(ph)), 7.14 (dt, J = 7.0, 1.9 Hz, 1H, C *H* ph), 7.15 (m, 2H, C *H* ph), 7.51 (m, 2H, C *H* pz(CH*) + C *H* ph), 8.28 (s, 1H, C *H* py). ^{13}C NMR (75 MHz, $CDCl_3$) δ: 10.8 (*C*H$_3$ py *p*-CH), 13.3 (*C*H$_3$ py *o*-CH), 16.1 (*C*H$_3$SR), 16.3 (*C*H$_3$SAr), 38.2 (*C*H$_2$), 60.0 (*C*H$_3$O), 62.9 (*C*H*), 106.6 (*C*H pz(ph)), 124.5 (*C*H ph), 125.3 (*C*H ph), 126.1 (*C* quat), 126.5 (*C* quat), 128.0 (*C*H ph), 129.7 (*C*H ph), 132.6 (*C* quat), 137.4 (*C* quat), 149.1 (*C*H pz(CH*)), 149.6 (*C* quat), 154.7 (*C* quat), 164.1 (*C* quat). ESI−MS (p.i., 50 V, CH_3OH, *m*/*z*, I%): 400.6, 100, $[L^bH]^+$. Anal. Calcd for $C_{21}H_{25}N_3OS_2$ (399.57): C, 63.12; H, 6.31; N, 10.52. Found: C, 63.31; H, 6.15; N, 10.33.

Synthesis of $[Cu(L^a)]_2(BF_4)_2$ ($\mathbf{a_2}(BF_4)_2$). A solution of $[Cu(CH_3CN)_4]BF_4$ (132 mg, 0.42 mmol) in dichloromethane (10 mL) was added to a solution of L^a (157 mg, 0.38 mmol) in dichloromethane (10 mL) at room temperature with stirring. After 1 h, the solution was concentrated to ∼5 mL under a vacuum; hexane was added (25 mL), and a colorless oil formed, which was triturated, filtered, and dried under a vacuum. A white powder was collected ($\mathbf{a_2}(BF_4)_2$, 147 mg, 0.13 mmol, 70%). Colorless crystals suitable for X-ray diffraction were obtained by stratification of hexane over a dichloromethane solution of the product, corresponding to $[Cu(L^a)]_2(BF_4)_2\cdot 2CH_2Cl_2$ ($\mathbf{a_2}(BF_4)_2\cdot 2CH_2Cl_2$). IR (cm^{-1}): 3125m, 2922m, 1591m, 1565m, 1476s, 1430s, 1366m, 1304m, 1264s, 1220w, ∼1060 vs br, 762s. ^{1}H NMR (300 MHz, CD_3CN) δ: 2.07 (s, 3H, C H_3SR), 2.24 (s, 3H C H_3 py *p*-CH), 2.26 (s, 3H, C H_3 py *o*-CH), 2.34 (m, 3H, C $H_2(SCH_3)$ + *H*CH(CH*)), 2.43 (s, 3H, C H_3SAr), 2.87 (m, 1H, *H*′CH(CH*)), 3.80 (s, 3H, C H_3O), 6.04 (dd, J = 9.9, 4.6 Hz, 1H, C *H**), 6.57 (d, J = 2.4 Hz, 1H, C *H* pz(ph)), 7.42 (m, 2H, C *H* ph), 7.54 (m, 2H, C *H* ph), 7.89 (d, J = 2.4 Hz, 1H, C *H* pz(CH*)), 8.31 (s, 1H, C *H* py). ESI−MS (p.i., 45 V, CH_3CN, *m*/*z*, I%): 476.2, 100, $[Cu(L^a)]^+$. ESI−MS (p.i., 39 V, CH_3OH, *m*/*z*, I%): 476.2, 100, $[Cu(L^a)]^+$. Anal. Calcd for $B_2C_{44}Cu_2F_8H_{54}N_6O_2S_4$ (1127.90): C, 46.85; H, 4.82; N, 7.45. Found: C, 47.24; H, 4.96; N, 7.18.

Synthesis of $[Cu(L^b)]_2(BF_4)_2$ ($\mathbf{b_2}(BF_4)_2$). The same procedure used to prepare $\mathbf{a_2}(BF_4)_2$ was applied by using L^b (160 mg, 0.40 mmol) instead of L^a and a different quantity of $[Cu(CH_3CN)_4]BF_4$ (139 mg, 0.44 mmol). A white powder was collected ($\mathbf{b_2}(BF_4)_2$, 170 mg, 0.15 mmol, 77%). Colorless crystals suitable for X-ray diffraction were obtained by cooling an acetonitrile/water solution of the product to 8 °C. IR (cm^{-1}): 3137 w, 3001 w, 2930 m, 1589 w, 1568 w, 1470 m, 1427 m, 1351 w, 1254 m, ∼1035 m br, 762 m. ^{1}H NMR (300 MHz, CD_3CN) δ: 2.16 (s, 3H, C H_3SR), 2.29 (s, 3H, C H_3 py o-CH), 2.30 (s, 3H, C H_3 py p-CH), 2.47 (s, 3H, C H_3SAr), 3.35 (dd, J = 14.5, 5.5 Hz, 1H, *H*CH(CH*)), 3.54 (dd, J = 14.4, 8.1 Hz, 1H, *H*′CH(CH*)), 3.84 (s, 3H, C H_3O), 6.01 (dd, J = 8.9, 5.9 Hz, 1H, C *H**), 6.64 (d, J = 2.4 Hz, 1H, C *H* pz(ph)), 7.46 (m, 2H, C *H* ph), 7.58 (m, 2H, C *H* ph), 7.98 (d, J = 2.4 Hz, 1H, C *H* pz(CH*)), 8.33 (s, 1H, C *H* py). ESI−MS (p.i., 54 V, CH_3CN, *m*/*z*, I%): 462.2, 100, $[Cu(L^b)]^+$. ESI−MS (p.i., 30 V, CH_2Cl_2, *m*/*z*, I%): 462.2, 100, $[Cu(L^b)]^+$. Anal. Calcd for $B_2C_{42}Cu_2F_8H_{50}N_6O_2S_4$ (1099.85): C, 45.86; H, 4.58; N, 7.64. Found: C, 45.61; H, 4.75; N, 7.80.

X-ray Crystallography. A summary of data collection and structure refinement for $\mathbf{a_2}(BF_4)_2\cdot 2CH_2Cl_2$ and $\mathbf{b_2}(BF_4)_2$ is reported in Table 1. Single-crystal data were collected with a Bruker Smart 1000 area detector diffractometer (Mo Kα; λ = 0.710 73 Å). Cell parameters were refined from the observed setting angles and detector positions of selected strong reflections. Intensities were integrated from several series of exposure frames that covered the sphere of reciprocal space.[17] No crystal decay was observed. An absorption correction was applied for $\mathbf{a_2}(BF_4)_2\cdot 2CH_2Cl_2$ and $\mathbf{b_2}(BF_4)_2$ using SADABS,[18] with minimum and maximum transmission factors of 0.703–1.000 for $\mathbf{a_2}(BF_4)_2\cdot 2CH_2Cl_2$ and 0.763–1.000 for $\mathbf{b_2}(BF_4)_2$. The structures were solved by direct methods (SIR97)[19] and refined with full-matrix least-squares (SHELXL-97),[20] using the Wingx software package.[21] Non-hydrogen atoms were refined anisotropically, and the hydrogen atoms were placed at their calculated positions. In $\mathbf{a_2}(BF_4)_2\cdot 2CH_2Cl_2$, the independent BF_4^- is disordered in two positions with site occupancy factors of ∼0.4 and ∼0.6, respectively, whereas in $\mathbf{b_2}(BF_4)_2$, one of the two independent BF_4^- molecules is disordered in three positions with site occupancy factors of 0.33 for each image. Molecular diagrams were prepared using Mercury CSD 2.0.[22]

Table 1. Summary of X-ray Crystallographic Data for $\mathbf{a_2}(BF_4)_2\cdot 2CH_2Cl_2$ and $\mathbf{b_2}(BF_4)_2$

	$\mathbf{a_2}(BF_4)_2\cdot 2CH_2Cl_2$	$\mathbf{b_2}(BF_4)_2$
empirical formula	$C_{46}H_{58}B_2Cl_4Cu_2F_8N_6O_2S_4$	$C_{42}H_{50}B_2Cu_2F_8N_6O_2S_4$
formula weight	1297.72	1099.82
color, habit	colorless, block	colorless, block
crystal size (mm)	0.45 × 0.35 × 0.23	0.25 × 0.20 × 0.15
crystal system	triclinic	monoclinic
space group	$P\bar{1}$	$P2_1/c$
a (Å)	10.548(1)	11.899(6)
b (Å)	12.138(1)	21.022(7)
c (Å)	12.780(1)	19.541(2)
α (deg)	111.20(1)	90
β (deg)	101.16(1)	91.14(2)
γ (deg)	101.29(2)	90
V (Å^3)	1432.1(2)	4887(3)
Z	1	4
T (K)	293(2)	293(2)
ρ (calcd) (Mg/m^3)	1.505	1.495
μ (mm^{-1})	1.143	1.114
θ range (deg)	1.79 to 28.07	1.71 to 26.00
number of reflections/ observed	16 171/3779	9588/4067
GooF	1.037	0.996
$R1^a$	0.0426	0.0597
$wR2^a$	0.0910	0.0816

^{a} $R1 = \Sigma||F_o| - |F_c||/\Sigma|F_o|$, $wR2 = [\Sigma[w(F_o^2 - F_c^2)^2]/\Sigma[w(F_o^2)^2]]^{1/2}$, $w = 1/[\sigma^2(F_o^2) + (aP)^2 + bP]$, where $P = [\max(F_o^2, 0) + 2F_c^2]/3$.

NMR Titrations. Dilution ^{1}H NMR titrations for $\mathbf{a_2}(BF_4)_2$ and $\mathbf{b_2}(BF_4)_2$ were performed at 280, 290, 300, and 310 K in CD_3CN. A total of 11 spectra were registered in the copper concentration (C_{Cu}) range of 0.1–0.000 14 M for each temperature. Tetramethylsilane (TMS) was used as the internal standard, and a line broadening factor of 0.5 was applied. The variation of the chemical shifts with dilution was used to determine the equilibrium constants of the dimerization processes. The refinement of the data was initially performed with the HypNMR 2006 program,[23] yielding stoichiometric constants (K). Because the ionic strength varies over

(17) *SMART (Control) and SAINT (Integration) Software for CCD Systems*; Bruker AXS: Madison, WI, 1994.
(18) *Area-Detector Absorption Correction*; Siemens Industrial Automation, Inc.: Madison, WI, 1996.
(19) Altomare, A.; Burla, M. C.; Camalli, M.; Cascarano, G. L.; Giacovazzo, C.; Guagliardi, A.; Moliterni, A. G. G.; Polidori, G.; Spagna, R. *J. Appl. Crystallogr.* **1999**, *32*, 115–119.
(20) Sheldrick, G. M. SHELX97. *Programs for Crystal Structure Analysis (Release 97-2)*; University of Göttingen: Göttingen, Germany, 1997.
(21) Farrugia, L. J. *J. Appl. Crystallogr.* **1999**, *32*, 837–838.
(22) Macrae, C. F.; Edgington, P. R.; McCabe, P.; Pidcock, E.; Shields, G. P.; Taylor, R.; Towler, M.; van de Streek, J. *J. Appl. Crystallogr.* **2006**, *39*, 453–457.
(23) Frassineti, C.; Ghelli, S.; Gans, P.; Sabatini, A.; Moruzzi, M. S.; Vacca, A. *Anal. Biochem.* **1995**, *231*, 374–382.

the course of the dilution, an empirical correction for ionic-strength variation was applied (Davies' equation),[24] yielding stability constants extrapolated at zero ionic strength (K^0) (Supporting Information). SPSS 15.0[25] was used to perform the van't Hoff analysis, which afforded the thermodynamic parameters for the dimerization equilibrium (ΔH^0 and ΔS^0). The distribution diagrams were calculated and plotted by HySS 2006.[26]

PGSE Experiments. ^{1}H PGSE NMR measurements were performed for $\mathbf{a_2}(BF_4)_2$ and $\mathbf{b_2}(BF_4)_2$ solutions in CD_3CN ($\epsilon = 37.5$ at 21 °C) at different C_{Cu} ($10^{-1}-10^{-4}$ M range), using a standard stimulated echo (STE) sequence on a Bruker Avance 300 spectrometer at 300 K without spinning. The most intense signals were investigated. The dependence of the resonance intensity (I) on the gradient strength (g) is described by the following equation:

$$I = I_0 e^{-D\gamma^2 g^2 \delta^2 (\Delta - \delta/3)}$$

where I is the observed intensity (attenuated signal intensity), I_0 is the reference intensity (unattenuated signal intensity), D is the diffusion coefficient, γ is the nucleus gyromagnetic ratio, g is the gradient strength, δ is the gradient duration, and Δ is the diffusion delay. The parameters δ and Δ were kept constant during the experiments, whereas g varied from 2 to 95% in 16 steps. Different values of δ (1–2 ms), Δ (50–100 ms), and number of scans (depending upon the concentration) were used for different samples. All spectra were acquired using 16 000 points and processed with a line broadening of 1.0 Hz. PGSE data were treated by applying a procedure reported in the literature,[27,28] taking advantage of an internal standard (tetrakismethylsilylsilane, TMSS; r_H^{TMSS} (hydrodynamic radius) $\approx r_{vdW}^{TMSS}$ (van der Waals radius) = 4.28 Å).[29] A nonlinear regression on I and g^2 data was performed with the SPSS 15.0 software to obtain the coefficients $m = D\gamma^2\delta^2(\Delta - \delta/3)$ for both the sample and the corresponding internal standard signals (m^{sample} and m^{TMSS}, respectively). The following expression (on the basis of the Stokes–Einstein equation) was applied and numerically resolved to get the hydrodynamic radius of each sample (r_H^{sample}):

$$\frac{c^{TMSS} r_H^{TMSS}}{c^{sample} r_H^{sample}} = \frac{m^{sample}}{m^{TMSS}}$$

The coefficients c^{sample} and c^{TMSS} can be estimated from the semiempirical equation[30]

$$c^x = \frac{6}{\left(1 + 0.695 \frac{r^{solv}}{r_H^x}\right)^{2.234}}$$

where x is the sample or TMSS, and $r^{solv} \approx$ van der Waals radius of the solvent (2.33 Å for CD_3CN). Hydrodynamic volumes were calculated from the respective radii: $V_H = {}^4/_3\pi(r_H)^3$. Uncertainties were obtained by error propagation on m.

The van der Waals volumes (V_{vdW})[31] and the Connolly volumes ($V_{Connolly}$)[32] were computed for both the X-ray ($\mathbf{a_2}^{2+}$ and $\mathbf{b_2}^{2+}$) and DFT optimized structures ($\mathbf{a}^+$ and $\mathbf{b}^+$) using the software package DS Viewer Pro 5.0. The X-ray volume ($V_{X\text{-}ray}$) was calculated by dividing the crystallographic unit cell volume by the number of molecular entities contained in the unit cell and subtracting the $V_{Connolly}$ of counterions and solvent.

DFT Calculations. DFT calculations were carried out with Gaussian 03.[33] The mononuclear models $[Cu(L^a)]^+$ ($\mathbf{a}^+$) and $[Cu(L^b)]^+$ ($\mathbf{b}^+$) were optimized starting from hypothetical tetrahedral Cu^I complexes, in which the ligands are *N*,*N*′,*S*,*S*′-coordinated. The B3LYP[34,35] density functional and the lanl2dz basis set with Hay and Wadt effective core potential (ECP) were employed.[36,37] Vibrational frequencies were calculated at the same theoretical level to ensure that the stationary points were true minima. As described in the PGSE section, the optimized geometries were used to determine the theoretical volumes, V_{vdW} and $V_{Connolly}$, which were compared to the hydrodynamic volumes extrapolated from PGSE NMR experiments.

Electrochemistry. Cyclic voltammetry (CV) was performed in a three-electrode cell with a Pt disk as the working electrode, a Pt rod as the counter-electrode, and a 3 M Ag/AgCl/KCl ($E^0 = +194$ mV, $T = 25$ °C) as the reference electrode, using a computerized electrochemical workstation consisting of an Autolab PGSTSAT 20 potentiostat (Ecochemie, Utrecht, The Netherlands) controlled by GPES 4.9 software. Cyclic voltammograms were recorded at different scan rates (20, 50, 100, 200, and 500 mV s^{-1}) on freshly prepared solutions of $\mathbf{a_2}(BF_4)_2$ and $\mathbf{b_2}(BF_4)_2$ in CH_2Cl_2 and CH_3CN at two different concentrations (0.01 and 0.001 M). All of the samples contained 0.1 M supporting electrolyte (tetra-*n*-butylammonium hexafluorophosphate, NBu_4PF_6).

Results and Discussion

The synthesis of L^a and L^b is described in Scheme 1. The reaction between 2-chloromethyl-4-methoxy-3,5-dimethylpyridine and 3-(2-(methylthio)phenyl)-1*H*-pyrazole affords the *N*,*N*′,*S* donor ligand, L, which can be functionalized on the methylene bridge with opportune electrophiles after deprotonation with *n*-butyllithium, in analogy to the preparation of bis(pyrazolyl)-scorpionates.[4c] The use of 2-chloroalkyl methyl sulfides provides good yields of the *N*,*N*′,*S*,*S*′ heteroscorpionate ligands L^a and L^b. To obtain a more symmetric N_2,*S*,*S*′ donor ligand, we first attempted the reaction between 3,5-alkyl-substituted bis(pyrazolyl)methanes (previously deprotonated with *n*-BuLi) and 2-chloromethyl methyl sulfide, but we recovered the parent bis(pyrazolyl)methanes

(24) Davies, C. W. *Ion Association*; Butterworth: Washington, D.C., 1962.
(25) SPSS, Inc. 1989–2006. All rights reserved.
(26) Alderighi, L.; Gans, P.; Ienco, A.; Peters, D.; Sabatini, A.; Vacca, A. *Coord. Chem. Rev.* **1999**, *184*, 311–318.
(27) Macchioni, A.; Ciancaleoni, G.; Zuccaccia, C.; Zuccaccia, D. *Chem. Soc. Rev.* **2008**, doi: 10.1039/b615067p, in press.
(28) Zuccaccia, D.; Macchioni, A. *Organometallics* **2005**, *24*, 3476–3486.
(29) Dinnebier, R. E.; Dollase, W. A.; Helluy, X.; Kummerlen, J.; Sebald, A.; Schmidt, M. U.; Pagola, S.; Stephens, P. W.; Van Smaalen, S. *Acta Crystallogr., Sect. B: Struct. Sci.* **1999**, *55*, 1014–1029.
(30) Chen, H. C.; Chen, S. H. *J. Phys. Chem.* **1984**, *88*, 5118–5121.
(31) Bondi, A. *J. Phys. Chem.* **1964**, *68*, 441–451.
(32) Connolly, M. L. *J. Am. Chem. Soc.* **1985**, *107*, 1118–1124.
(33) Frisch, M J.; Trucks, G. W.; Schlegel, H. B.; Scuseria, G. E.; Robb, M. A.; Cheeseman, J. R.; Montgomery, J. A., Jr.; Vreven, T.; Kudin, K. N.; Burant, J. C.; Millam, J. M.; Iyengar, S. S.; Tomasi, J.; Barone, V.; Mennucci, B.; Cossi, M.; Scalmani, G.; Rega, N.; Petersson, G. A.; Nakatsuji, H.; Hada, M.; Ehara, M.; Toyota, K.; Fukuda, R.; Hasegawa, J.; Ishida, M.; Nakajima, T.; Honda, Y.; Kitao, O.; Nakai, H.; Klene, M.; Li, X.; Knox, J. E.; Hratchian, H. P.; Cross, J. B.; Bakken, V.; Adamo, C.; Jaramillo, J.; Gomperts, R.; Stratmann, R. E.; Yazyev, O.; Austin, A. J.; Cammi, R.; Pomelli, C.; Ochterski, J. W.; Ayala, P. Y.; Morokuma, K.; Voth, G. A.; Salvador, P.; Dannenberg, J. J.; Zakrzewski, V. G.; Dapprich, S.; Daniels, A. D.; Strain, M. C.; Farkas, O.; Malick, D. K.; Rabuck, A. D.; Raghavachari, K.; Foresman, J. B.; Ortiz, J. V.; Cui, Q.; Baboul, A. G.; Clifford, S.; Cioslowski, J.; Stefanov, B. B.; Liu, G.; Liashenko, A.; Piskorz, P.; Komaromi, I.; Martin, R. L.; Fox, D. J.; Keith, T.; Al-Laham, M. A.; Peng, C. Y.; Nanayakkara, A.; Challacombe, M.; Gill, P. M. W.; Johnson, B.; Chen, W.; Wong, M. W.; Gonzalez, C.; Pople, J. A. *Gaussian 03, Revision C.02*; Gaussian, Inc.: Wallingford, CT, 2004.
(34) Becke, A. D. *Phys. Rev. A: At., Mol., Opt. Phys.* **1988**, *38*, 3098–3100.
(35) Becke, A. D. *J. Chem. Phys.* **1993**, *98*, 5648–5652.
(36) Hay, P. J.; Wadt, W. R. *J. Chem. Phys.* **1985**, *82*, 299–310.
(37) Wadt, W. R.; Hay, P. J. *J. Chem. Phys.* **1985**, *82*, 284–298.

Scheme 2

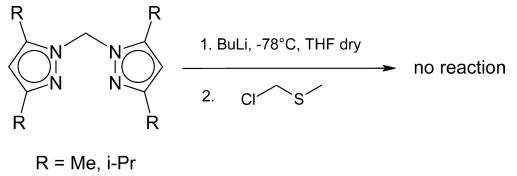

instead of the desired product (Scheme 2). With respect to the preparation of L^{a} and L^{b}, the presence of the pyridyl group confers a greater stability to the benzylic carbanion, therefore allowing for the attack of weak acid electrophiles. L^{a} and L^{b} are chiral ligands because of the asymmetry of the central carbon atom, and we did not attempt to resolve the racemic mixture, which was then employed for the preparation of the copper complexes. As far as the coordination capabilities of the ligands are concerned, the two thioether moieties and the pyrazole−pyridine assembly could provide the N_2S_2 coordination mode required by Cu^{I} in a hypothetical mononuclear complex. Nevertheless, when reacting L^{a} with $[Cu(CH_3CN)_4]BF_4$, the dinuclear complex $\mathbf{a_2}(BF_4)_2$ was obtained, probably because of the extreme flexibility of the alkyl thioether arm of L^{a}. To reduce the degrees of freedom of this fourth donor group, we reduced the length of the alkyl chain from $-CH_2-CH_2SCH_3$ to $-CH_2-SCH_3$ (in L^{b}) but with no substantial changes in the coordination properties of the ligand or in the geometry of the resulting complex. In fact, from a Cu^{I} coordination perspective, $\mathbf{b_2}(BF_4)_2$ is identical to $\mathbf{a_2}(BF_4)_2$.

The two complexes are soluble in acetonitrile, nitromethane, and dichloromethane and slightly soluble in acetone. If dichloromethane solutions of $\mathbf{a_2}(BF_4)_2$ and $\mathbf{b_2}(BF_4)_2$ are exposed to air, after some time, they turn green as a consequence of copper(I) oxidation; in the case of $\mathbf{b_2}(BF_4)_2$, green crystals of the oxidized product $[Cu(L^b)Cl_2]$ were isolated. On the other hand, the complex $[Cu(L^a)_2(H_2O)](OTf)_2$ (OTf^- = triflate) was prepared by reacting $Cu(OTf)_2$ and L^{a} in 1:1 molar ratio in methanol. These complexes may be taken as models for the coordination capabilities of the ligands with Cu^{II} (see below).

Solid-State Structures. Relevant geometric parameters of $\mathbf{a_2}(BF_4)_2$ and $\mathbf{b_2}(BF_4)_2$ are listed in Table 2. Both compounds exhibit a dinuclear structure, presenting an almost equivalent metal coordination geometry (Figures 1 and 2). Each Cu^{I} is located in a distorted tetrahedral environment, bound by two nitrogen atoms and the aryl-thioether sulfur atom of a ligand, with the fourth coordination site deriving from the alkyl-thioether sulfur atom of the second ligand. The Cu−N bond distances are nearly equivalent for both compounds (2.040(2)−2.001(2) Å in $\mathbf{a_2}(BF_4)_2$ and 2.076(4)−2.034(4) Å in $\mathbf{b_2}(BF_4)_2$). The bridging alkyl-thioether group gives rise to Cu−S bond distances that are significantly shorter (with differences that vary from ∼0.10 and ∼0.25 Å) than those derived from the aryl thioether. The reason for this may reside in the better donor ability of the alkyl-thioether with respect to the aryl-thioether, but it could also be a consequence of the major stereochemical constraints of the aryl-thioether, which results in a nonideal overlap of the coordinating lone pair of the sulfur with copper(I). $\mathbf{a_2}(BF_4)_2$ is centrosymmetric, with the

Table 2. Selected Bond Lengths (Å) and Angles (deg) for $\mathbf{a_2}(BF_4)_2\cdot 2CH_2Cl_2$ and $\mathbf{b_2}(BF_4)_2$

	$\mathbf{a_2}(BF_4)_2\cdot 2CH_2Cl_2$		
Cu−S(11)	2.452(1)	Cu−N(13)	2.040(2)
Cu−S(12)^{a}	2.201(1)	Cu−N(21)	2.001(2)
N(21)−Cu−N(13)	92.27(9)	S(12)′−Cu−S(11)	109.82(3)
N(21)−Cu−S(12)^{a}	128.14(7)	N(13)−Cu−S(12)^{a}	123.17(7)
N(21)−Cu−S(11)	87.81(7)	N(13)−Cu−S(11)	109.74(7)
	$\mathbf{b_2}(BF_4)_2$		
Cu(1)−S(11)	2.335(2)	Cu(2)−S(12)	2.239(2)
Cu(1)−S(15)	2.246(2)	Cu(2)−S(14)	2.302(2)
Cu(1)−N(21)	2.044(4)	Cu(2)−N(24)	2.034(4)
Cu(1)−N(13)	2.076(4)	Cu(2)−N(16)	2.071(4)
N(21)−Cu(1)−N(13)	90.1(2)	N(24)−Cu(2)−N(16)	90.9(2)
N(21)−Cu(1)−S(15)	124.0(1)	N(24)−Cu(2)−S(12)	123.8(1)
N(13)−Cu(1)−S(15)	117.3(1)	N(16)−Cu(2)−S(12)	118.6(1)
N(21)−Cu(1)−S(11)	85.6(1)	N(24)−Cu(2)−S(14)	93.7(1)
N(13)−Cu(1)−S(11)	113.5(1)	N(16)−Cu(2)−S(14)	114.5(1)
S(15)−Cu(1)−S(11)	119.35(6)	S(12)−Cu(2)−S(14)	111.89(6)

^{a} $-x+1$, $-y$, and $-z+1$.

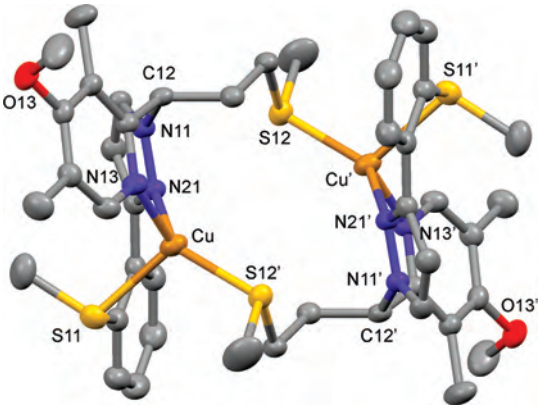

Figure 1. Molecular drawing of $\mathbf{a_2}(BF_4)_2\cdot 2CH_2Cl_2$ at the 30% thermal ellipsoid probability level. The BF_4^- counterions, the hydrogen atoms, and the crystallization solvent molecules are omitted for clarity. ′ = $1-x$, $-y$, and $1-z$.

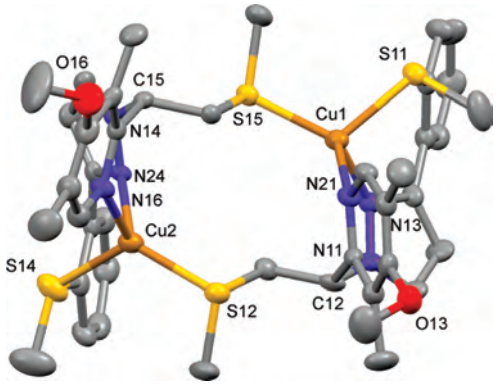

Figure 2. Molecular drawing of $\mathbf{b_2}(BF_4)_2$ at the 30% thermal ellipsoid probability level. The BF_4^- counterions and the hydrogen atoms are omitted for clarity.

two ligands presenting the stereogenic carbon in the *R* and *S* configurations, respectively. In $\mathbf{b_2}(BF_4)_2$, the ligands exhibit equivalent configurations for the central carbon, so that the complex is asymmetric; however, because the space group is centrosymmetric ($P2_1/c$) both *R*,*R* and *S*,*S* enantiomers are present in the unit cell. In addition, the metals are also stereogenic centers, and in $\mathbf{a_2}(BF_4)_2$, they exhibit opposite chirality (because of the center of symmetry), whereas in

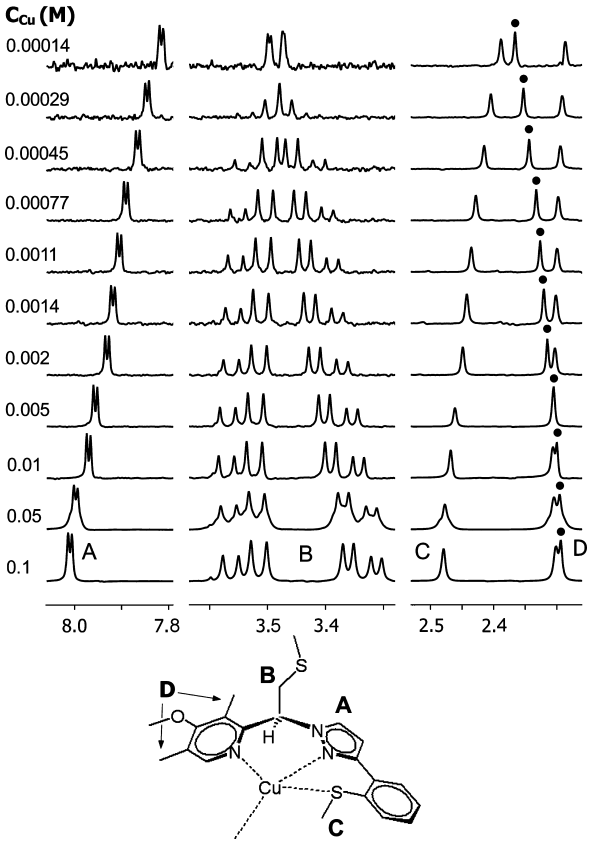

Figure 3. Stacking plot of ^{1}H NMR spectra of $\mathbf{b_2}(BF_4)_2$ in CD_3CN at different copper concentrations (C_{Cu}). The drifts of the A, C, and D chemical shifts were used to derive the log K^0 for the $2\mathbf{b}^+ = \mathbf{b_2}^{2+}$ equilibrium.

$\mathbf{b_2}(BF_4)_2$, they adopt the same configuration. In summary, the overall chirality of $\mathbf{a_2}(BF_4)_2$ can be represented as $(R,S)_C(R,S)_{Cu}$, whereas that of $\mathbf{b_2}(BF_4)_2$ can be represented as $(R,R)_C(R,R)_{Cu}/(S,S)_C(S,S)_{Cu}$. The large distance between the two copper centers (4.972(1) Å in $\mathbf{a_2}(BF_4)_2$ and 5.212(2) Å $\mathbf{b_2}(BF_4)_2$) rules out any metal−metal interaction.

The crystal structures of the Cu^{II} complexes $[Cu(L^b)Cl_2]$ and $[Cu(L^a)_2(H_2O)](OTf)_2$ are reported in Figures S1 and S2 of the Supporting Information. In both structures, the metal exhibits a trigonal bipyramidal geometry. In $[Cu(L^b)Cl_2]$, the metal is bound to a κ^3-*N*,*N*′,*S* ligand and two chloride ions. The apical positions are occupied by the aryl-thioether sulfur and the pyridine nitrogen, whereas the pyrazole nitrogen atom and two chloride ions are in the equatorial plane. The alkyl-thioether sulfur does not take part in the metal coordination. In $[Cu(L^a)_2(H_2O)](OTf)_2$, the metal is bound by two k^2-*N*,*N*′ ligands, with both thioether groups not coordinated. The pyridine nitrogen atoms are in apical positions, whereas the pyrazole nitrogen atom and a water molecule occupy the equatorial positions.

Solution Studies. To better comprehend the solution behavior of the complexes, we performed dilution ^{1}H NMR titrations for $\mathbf{a_2}(BF_4)_2$ and $\mathbf{b_2}(BF_4)_2$ in CD_3CN. In both cases, when the analytical copper concentration (C_{Cu}) was varied, we observed a drift in the chemical shift of various protons. In Figure 3 and Figure S3 of the Supporting Information, the NMR stacking plots of $\mathbf{b_2}(BF_4)_2$ and $\mathbf{a_2}(BF_4)_2$ are reported. In addition, the diastereotopic methylene protons of $\mathbf{b_2}(BF_4)_2$ (peak B in Figure 3), constituting an ABX spin

Table 3. Logarithms of the Zero Ionic Strength Equilibrium Constants (log K^0) for the Dimerization Processes $2\mathbf{a}^+ = \mathbf{a_2}^{2+}$ and $2\mathbf{b}^+ = \mathbf{b_2}^{2+}$ in the 280–310 K Temperature Range

T (K)	log K^0 ($\mathbf{a_2}^{2+}$)	log K^0 ($\mathbf{b_2}^{2+}$)
280	3.70(10)	3.36(6)
290	3.65(7)	3.27(5)
300	3.55(6)	3.23(5)
310	3.48(5)	3.17(4)

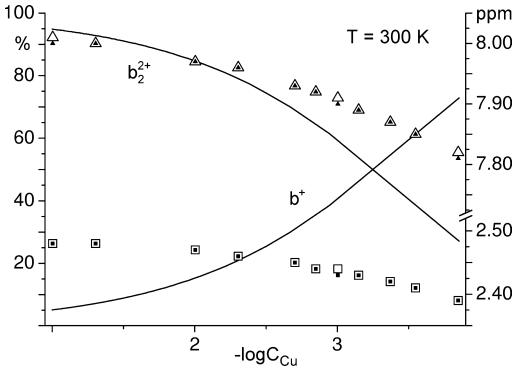

Figure 4. Distribution diagram corresponding to the dilution ^{1}H NMR titration of $\mathbf{b_2}(BF_4)_2$ in CD_3CN at 300 K (C_{Cu} = copper concentration). The observed and calculated chemical shifts for peaks A (△, ▲) and C (□, ■) of Figure 3 are reported.

system, exhibit two doublets of doublets in concentrated solution, whereas in dilute solutions ($C_{Cu} \approx 10^{-4}$ M), they give rise to a pseudo-doublet. This phenomenon can be explained with the gradual appearance, over the course of dilution, of a fast-exchanging species that is less "aggregated" than the complex predominant at high C_{Cu} (presumably the dinuclear complex) and whose methylene protons have closer chemical shifts, so that a pseudo-doublet appears for second-order effects. This is in accordance with the presence of a fast monomer–dimer equilibrium, which would also explain the variation of the chemical shifts of the other protons. To exclude the possibility that this behavior is related to the aggregation of cations and anions in solution (ion pairing),[38] BF_4^- was substituted with BPh_4^-, providing the complex $\mathbf{b_2}(BPh_4)_2$.[39] The trend of the NMR spectra at three different C_{Cu} (Figure S4 of the Supporting Information) is analogous to that of $\mathbf{b_2}(BF_4)_2$ and would rule out the ion-pairing hypothesis. These conclusions can be extended to $\mathbf{a_2}(BF_4)_2$. Moreover, in other solvents (CD_3NO_2, $(CD_3)_2CO$, and CD_2Cl_2) the complexes present spectral characteristics similar to the ones previously described, even though the spectra are much less resolved (data not reported). The equilibrium constants of the association processes, $2\mathbf{a}^+ = \mathbf{a_2}^{2+}$ and $2\mathbf{b}^+ = \mathbf{b_2}^{2+}$, were determined in CD_3CN at different temperatures (280−310 K, Table 3).

The distribution diagram of $\mathbf{b_2}^{2+}$ at 300 K is reported in Figure 4, together with the variation in selected observed and calculated chemical shifts as a function of C_{Cu}; in a 10^{-4} M solution, the monomer/dimer ratio is ∼9:1, whereas in a

(38) Macchioni, A. *Chem. Rev.* **2005**, *105*, 2039–2073.
(39) To a white suspension of $\mathbf{b_2}(BF_4)_2$ in THF, $KBPh_4$ was added in an equimolar ratio with stirring. The solid was filtered off, and the resulting clear yellow solution was concentrated. A creamy white powder was precipitated with hexane and dried under vacuum, corresponding to $\mathbf{b_2}(BPh_4)_2$.

10^{-1} M solution, this ratio is nearly reversed. The distribution diagrams obtained at different temperatures (also for $\mathbf{a_2}^{2+}$) are reported in Figures S5−S11 of the Supporting Information. By means of a van't Hoff analysis (Figures S12 and S13 of the Supporting Information), the thermodynamic parameters of the dimerization processes were determined; the ΔH^0 values show that both reactions are slightly exothermic ($\Delta H^0(\mathbf{a_2}^{2+}) = -12(1)$ kJ mol^{-1}, $\Delta H^0(\mathbf{b_2}^{2+}) = -10(1)$ kJ mol^{-1}), while the ΔS^0 are surprisingly positive ($\Delta S^0(\mathbf{a_2}^{2+}) = +27(4)$ kJ mol^{-1}, $\Delta S^0(\mathbf{b_2}^{2+}) = +28(4)$ kJ mol^{-1}). The small ΔH^0 values can be justified by considering that there is no net bond formation or rupture in these monomer/dimer equilibria, because two Cu^{I}−S(thioether) dissociations are compensated by two Cu^{I}−S(thioether) formations. Furthermore, the hypothesis that acetonitrile would complete the coordination of copper in the monomer in place of a thioether group of L^{a} or L^{b} can be excluded by taking into account the energetics of the model reaction, $[Cu(MeCN)_2]^+ + 2Me_2S = [Cu(Me_2S)_2]^+ + 2MeCN$ (+30.1 kJ mol^{-1}),[40] from which it is evident that the substitution of acetonitrile bound at Cu^{I} with a thioether is an unfavorable process. In the present case, given the exothermic nature of the dimerization, we can assume that no CH_3CN molecules are liberated in the reaction; hence, the ligands would behave as κ^4-*N*,*N*′,*S*,*S*′ tetradentate in the monomers. The entropy values deserve some comments, even though it has to be kept in mind that the determination of ΔS^0 through a van't Hoff analysis is affected by an intrinsic limited accuracy. In the present case, the positive ΔS^0 of dimerization can be justified with a better overall solvation of the monomers with respect to the dinuclear entities, resulting in the release of solvent molecules during the association.[41–44]

To propose a molecular geometry for the mononuclear complexes, $\mathbf{a}^+$ and $\mathbf{b}^+$, density functional theory (DFT) calculations were performed and the optimized structures are reported in Figure 5. It appears that both L^{a} and L^{b} can accommodate Cu^{I}, even if in a considerably distorted tetrahedral, almost bisphenoidal, environment. In particular, the S−Cu−S angle in $\mathbf{a}^+$ and $\mathbf{b}^+$ is significantly greater than that in $\mathbf{a_2}^{2+}$ and $\mathbf{b_2}^{2+}$ (Figure 6). In the monomers, the most relevant structural consequence that is derived from the different length of the alkyl-thioether arm is in a more pronounced coordination strain at the metal in $\mathbf{b}^+$ with respect to $\mathbf{a}^+$, with a consequent increase in the S−Cu−S angle by ∼10°. This is also associated with a slight increase of the Cu−S_{alkyl} bond length by ∼0.04 Å.

From the analysis of the log K^0 values, it appears that $\mathbf{a}^+$ exhibits a slightly greater propensity to dimerize if compared to $\mathbf{b}^+$; conversely, $\mathbf{b_2}^{2+}$ is more easily dissociated into monomers with respect to $\mathbf{a_2}^{2+}$. This can be tentatively

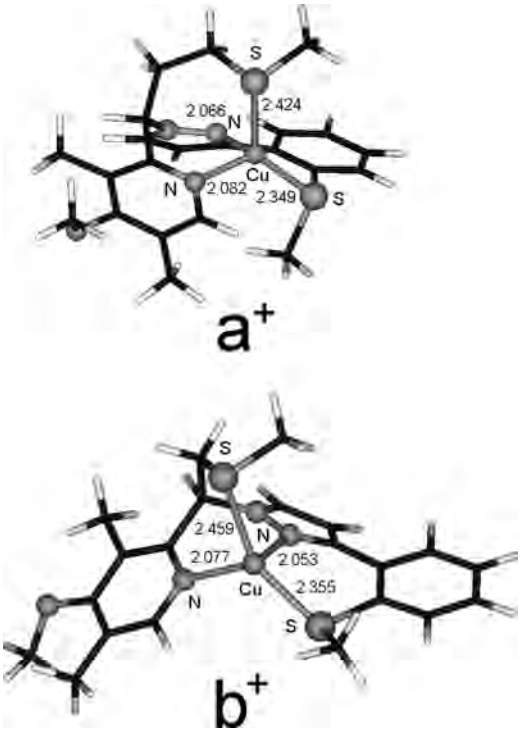

Figure 5. DFT-optimized geometries (B3LYP/lanl2dz) of the cationic mononuclear species $\mathbf{a}^+$ and $\mathbf{b}^+$.

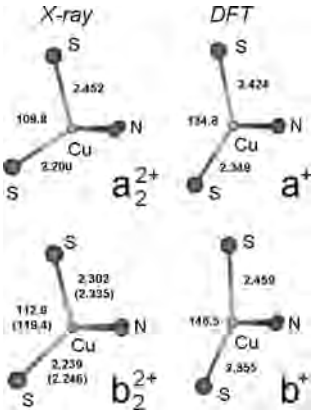

Figure 6. Comparison between the Cu^{I} experimental geometries (X-ray) of the dinuclear complexes $\mathbf{a_2}^{2+}$ and $\mathbf{b_2}^{2+}$ with the respective DFT-optimized mononuclear species $\mathbf{a}^+$ and $\mathbf{b}^+$. The double values in $\mathbf{b_2}^{2+}$ reflect the two different metal geometries as found in the crystal structure.

explained by a close inspection of Figures 5 and 6, where the Cu^{I} geometry of the di- and mononuclear species (as derived by X-ray analysis and DFT calculations, respectively) is compared. In fact, in the mononuclear complex, the alkyl-thioether in L^{a} gives rise to two seven-member chelate rings and a six-member one, whereas in L^{b}, it generates three six-member chelate rings and thus a more stable mononuclear complex.

As far as the kinetics of the dimerization process are concerned, the fast-exchange regime is in agreement with the lability of the Cu^{I}−S(thioether) bonds and with the low viscosity of acetonitrile (3.69×10^{-4} Pa s at 298 K). A variable-temperature NMR experiment was performed on a 0.000 45 M sample of $\mathbf{b_2}(BF_4)_2$ in CD_3CN (wherein the dimer and monomer are about at equimolar ratio) in the 300−230

(40) Deng, H. T.; Kebarle, P. *J. Am. Chem. Soc.* **1998**, *120*, 2925–2931.
(41) Berger, M.; Schmidtchen, F. P. *Angew. Chem., Int. Ed.* **1998**, *37*, 2694–2696.
(42) Fiammengo, R.; Timmerman, P.; de Jong, F.; Reinhoudt, D. N. *Chem. Commun.* **2000**, *2313*, 2314.
(43) Linton, B. R.; Goodman, M. S.; Fan, E.; van Arman, S. A.; Hamilton, A. D. *J. Org. Chem.* **2001**, *66*, 7313–7319.
(44) Corbellini, F.; Fiammengo, R.; Timmerman, P.; Crego-Calama, M.; Versluis, K.; Heck, A. J. R.; Luyten, I.; Reinhoudt, D. N. *J. Am. Chem. Soc.* **2002**, *124*, 6569–6575.

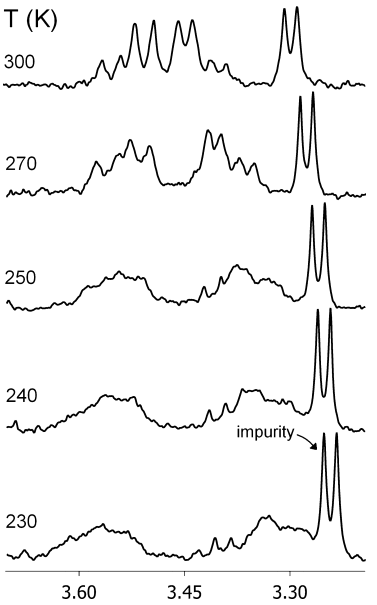

Figure 7. Variable temperature ^{1}H NMR of a $\mathbf{b_2}(BF_4)_2$ solution (C_{Cu} = 0.000 45 M) in CD_3CN. B protons are shown (see Figure 3).

Table 4. Experimental Hydrodynamic Volumes (V_H) for $\mathbf{a_2}(BF_4)_2$ and $\mathbf{b_2}$ $(BF_4)_2$ in CD_3CN at Different Copper Concentrations (C_{Cu}) at 300 K

C_{Cu} (M)	V_H ($\mathbf{a_2}(BF_4)_2$) (Å^3)	V_H ($\mathbf{b_2}(BF_4)_2$) (Å^3)
0.0001	700(20)	590(20)
0.001	780(20)	700(20)
0.01	860(30)	820(20)
0.1	950(30)	860(30)

K range. Upon decreasing the temperature, an enlargement of the signals can be noted; this is particularly evident for the methylene protons (Figure 7). However, the kinetic parameters could not be determined through a complete line shape analysis because of the slight broadening of all of the peaks and the inability to estimate the chemical shifts of the single species below the temperature of coalescence.

To further confirm the dissociation of the dimers in solution and to determine the hydrodynamic volumes of both the monomers ($\mathbf{a}^+$ and $\mathbf{b}^+$) and the dimers ($\mathbf{a_2}^{2+}$ and $\mathbf{b_2}^{2+}$), ^{1}H PGSE NMR experiments were performed on solutions of $\mathbf{a_2}(BF_4)_2$ and $\mathbf{b_2}(BF_4)_2$ at different C_{Cu} in CD_3CN (Table 4), and the data were interpolated for ideal monomer–dimer equilibria (Figure 8). The high permittivity of acetonitrile allows for the exclusion of ionic aggregation of all of the cationic complexes with BF_4^- anions,[45,46] which would not however affect the experimental hydrodynamic volumes because of the small encumbrance of BF_4^- (V_{vdW} = ~40 Å). For an ideal monomer–dimer equilibrium, the following equation can be derived (see the Supporting Information):

$$V_H = \left[\left(V_H^0(D) - 2V_H^0(M)\right)\left(\sqrt{8K^0C_{Cu}+1} - 4K^0C_{Cu}V_H^0(D) - V_H^0(D) + 2V_H^0(M)\right)\right] \Big/ \left(\sqrt{8K^0C_{Cu}+1} + 4K^0C_{Cu} - 1\right) \quad (1)$$

where V_H is the experimental hydrodynamic volume, $V_H^0(D)$ is the hydrodynamic volume of the dimer, $V_H^0(M)$ is the hydrodynamic volume of the monomer, and K^0 is the corrected dimerization constant (obtained from ^{1}H NMR titrations). The fitting with the experimental data is shown in Figure 8, whereas the hydrodynamic values of the individual species are reported in Table 5. For both complexes, $V_H^0(D)$ have values that lie between V_{vdW} and $V_{X\text{-}ray}$.[27] This latter volume is comparable to the solvent-excluded volume ($V_{Connolly}$) that is computed by taking into account the cavities and inlets of the solute, which are not accessible by the solvent (so that $V_{Connolly} > V_{vdW}$). As far as the monomers are concerned, in this case, $V_H^0(M)$ is also intermediate between V_{vdW} and $V_{Connolly}$. This is in agreement with previous results, which show that V_{vdW} and $V_{X\text{-}ray}/V_{Connolly}$ are the lower and upper limits of the real hydrodynamic volume.[27]

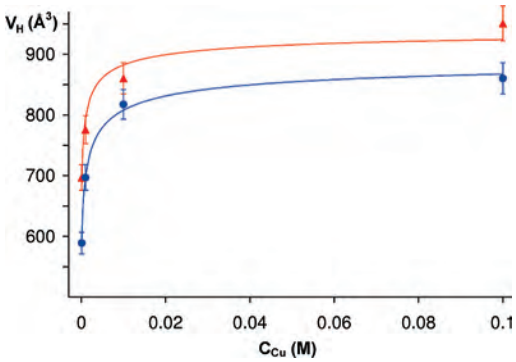

Figure 8. Experimental hydrodynamic volumes (V_H) of $\mathbf{a_2}(BF_4)_2$ (▲) and $\mathbf{b_2}(BF_4)_2$ (●) in CD_3CN plotted as a function of C_{Cu} at 300 K. The fitting curves, calculated according to eq 1, are reported.

Table 5. Hydrodynamic Volumes (V_H^0) of the Dimeric ($\mathbf{a_2}^{2+}$ and $\mathbf{b_2}^{2+}$) and Monomeric ($\mathbf{a}^+$ and $\mathbf{b}^+$) Species in CD_3CN, together with the van der Waals (V_{vdW}), Connolly ($V_{Connolly}$), and X-ray ($V_{X\text{-}ray}$) Volumes

	V_H^0 (Å^3)	V_{vdW} (Å^3)	$V_{Connolly}$ (Å^3)	$V_{X\text{-}ray}$ (Å^3)
$\mathbf{a_2}^{2+}$	950(20)	702	1339	1092
$\mathbf{a}^+$	620(40)	373	642	
$\mathbf{b_2}^{2+}$	900(10)	669	1280	1061
$\mathbf{b}^+$	550(10)	357	612	

An additional proof of the predominance of the monomeric species in diluted solution comes from the ESI−mass spectra (10^{-6} M solutions of $\mathbf{a_2}(BF_4)_2$ in CH_3CN and CH_3OH and $\mathbf{b_2}(BF_4)_2$ in CH_3CN and CH_2Cl_2), which show only the presence of monomers ($[L^{a/b}Cu]^+$ for both complexes) and without solvent molecules bound to copper.

Electrochemistry. The cyclic voltammograms of the 0.01 and 0.001 M solutions of $\mathbf{a_2}(BF_4)_2$ in CH_2Cl_2 and CH_3CN are reported in Figures 9 and 10, whereas those of the analogous solutions of $\mathbf{b_2}(BF_4)_2$ are depicted in Figures S14−S17 of the Supporting Information. The voltammetric parameters of the complexes are reported in Tables 6 and 7. CV experiments were also performed on 10^{-4} M solutions, but the voltammograms are not reported because the peaks are hardly detectable. In a first stage, the potential range employed allowed us to identify two redox systems for each sample: Cu^0/Cu^I and Cu^I/Cu^{II} couples. The former, in the $Cu^0 \rightarrow Cu^I$ process, was characterized by high peak current and a narrow shape typical of Cu^0 deposition on the electrode

(45) Pregosin, P. S. *Prog. Nucl. Magn. Reson. Spectrosc.* **2006**, *49*, 261–288.
(46) Zuccaccia, D.; Bellachioma, G.; Cardaci, G.; Ciancaleoni, G.; Zuccaccia, C.; Clot, E.; Macchioni, A. *Organometallics* **2007**, *26*, 3930–3946.

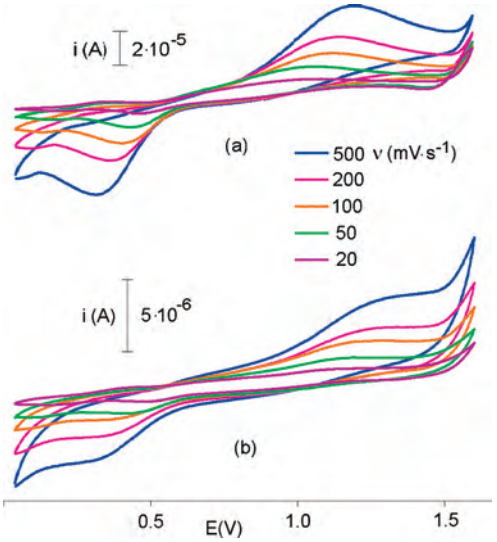

Figure 9. Cyclic voltammograms of $\mathbf{a_2}(BF_4)_2$ in CH_3CN at different scan rates (ν = 20−500 mV s^{-1}, third scans). (a) C_{Cu} = 0.01 M. (b) C_{Cu} = 0.001 M. Supporting electrolyte, 0.1 M NBu_4PF_6; reference electrode, 3 M Ag/AgCl/KCl.

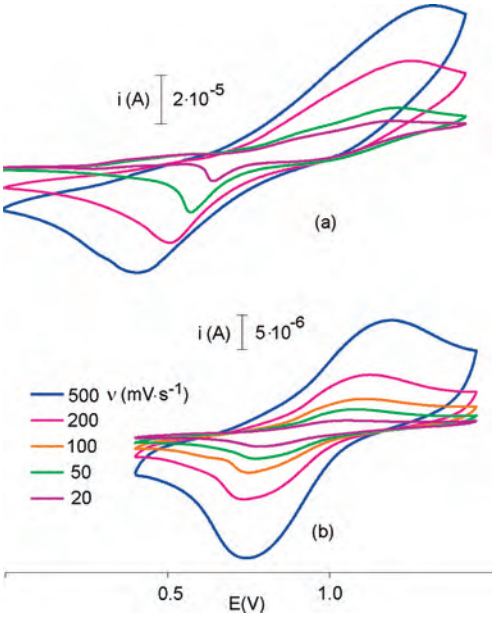

Figure 10. Cyclic voltammograms of $\mathbf{a_2}(BF_4)_2$ in CH_2Cl_2 at different scan rates (ν = 20−500 mV s^1, third scans). (a) C_{Cu} = 0.01 M. (b) C_{Cu} = 0.001 M. Supporting electrolyte, 0.1 M NBu_4PF_6; reference electrode, 3 M Ag/AgCl/KCl.

surface ("anodic stripping").[47] The $Cu^0 \rightarrow Cu^I$ oxidation generates a Cu^I species that may be different from the initial Cu^I complex. To avoid such an electrochemical process, the lower limit of the potential window was set at higher values; hence, the reported voltammograms depict only the Cu^I/Cu^{II} redox system.

The complexes show quasi-reversible to irreversible redox behavior of the Cu^I/Cu^{II} couple in all of the experimental conditions (e.g., solvent and concentration); in fact, the separation between the forward (anodic, E_{pa}) and reverse (cathodic, E_{pc}) peaks always increases with the scan rate (ν).

(47) Zanello, P. *Inorganic Electrochemistry: Theory, Practice and Application*; Royal Society of Chemistry: Cambridge, U.K., 2003.

Table 6. Summary of CV Parameters for $\mathbf{a_2}(BF_4)_2$ in CH_2Cl_2 and CH_3CN at C_{Cu} = 0.01 and 0.001 M

concentration (M)/solvent	ν (mV s^{-1})	E_{pa} (mV)	E_{pc} (mV)	ΔE_p (mV)	i_{pa}/i_{pc}
0.01/CH_2Cl_2	20	1.16	0.637	0.523	0.40
	50	1.157	0.569	0.588	0.46
	200	1.179	0.508	0.671	0.54
	500	1.223	0.42	0.803	0.45
0.001/CH_2Cl_2	20	1.02	0.793	0.227	0.58
	50	1.057	0.781	0.276	0.66
	100	1.076	0.754	0.322	0.61
	200	1.096	0.749	0.347	0.65
	500	1.154	0.759	0.395	0.55
0.01/CH_3CN	50	1.024	0.445	0.579	0.98
	100	1.087	0.421	0.666	1.02
	200	1.114	0.384	0.73	1.07
	500	1.161	0.343	0.818	1.00
0.001/CH_3CN	20	1.124	0.492	0.632	0.66
	50	1.185	0.457	0.728	0.72
	100	1.175	0.411	0.764	1.53
	200	1.214	0.389	0.825	1.10
	500	1.244	0.348	0.896	0.98

[a] ν, scan rate; E_{pa}, anodic peak potential; E_{pc}, cathodic peak potential; $\Delta E_p = E_{pa} - E_{pc}$; i_{pa}, anodic current; i_{pc}, cathodic current.

Table 7. Summary of CV Parameters for $\mathbf{b_2}(BF_4)_2$ in CH_2Cl_2 and CH_3CN at C_{Cu} = 0.01 and 0.001 M

concentration (M)/solvent	ν (mV s^{-1})	E_{pa} (mV)	E_{pc} (mV)	ΔE_p (mV)	i_{pa}/i_{pc}
0.01/CH_2Cl_2	50	1.201	0.505	0.696	0.85
	100	1.245	0.447	0.798	0.85
	200	1.272	0.408	0.864	0.84
	500	1.377	0.332	1.045	0.86
0.001/CH_2Cl_2	50	1.108	0.527	0.581	0.82
	100	1.111	0.503	0.608	0.81
	200	1.133	0.469	0.664	0.80
	500	1.243	0.4	0.843	0.82
0.01/CH_3CN	20	0.981	0.376	0.605	0.68
	50	1.174	0.293	0.881	0.73
	100	1.138	0.285	0.853	0.71
	200	1.199	0.244	0.955	0.72
	500	1.265	0.2	1.065	0.73
0.001/CH_3CN	50	1.108	0.398	0.71	0.75
	100	1.174	0.339	0.835	0.76
	200	1.211	0.327	0.884	0.77
	500	1.235	0.286	0.949	0.76

[a] ν, scan rate; E_{pa}, anodic peak potential; E_{pc}, cathodic peak potential; $\Delta E_p = E_{pa} - E_{pc}$; i_{pa}, anodic current; i_{pc}, cathodic current.

Nevertheless, the ΔE_p values ($E_{pa} - E_{pc}$) are considerably large, implying a high reorganization energy involved in the electron transfer.[48] This is tentatively justified with the flexibility of the ligands and, in particular, that of their alkylthioether "arm". This allows the electrogenerated Cu^{II} to organize the coordination sphere according to its electronic and steric preferences; i.e., to adopt five or six coordinations, as supported by the crystal structures of Cu^{II} with L^a and L^b (see Figures S1 and S2 of the Supporting Information). The analysis of these Cu^{II} complexes supports the hypothesis that the thioether groups may not be bound to Cu^{II}, so that the coordination/decoordination may contribute to the nonreversible behavior of the complexes. Moreover, the voltammetric behavior of the Cu^I systems is complicated by the dimerization equilibrium preceding the redox event, which reasonably involves two electroactive species (monomer and dimer). It is worth noting that, in the dimers, the two metal centers are electrochemically independent because of the

(48) Zanello, P. *Comm. Inorg. Chem.* **1988**, *8*, 45–78.

large distance between them (~5 Å). Bearing in mind that the Cu^{I} coordination sphere is equivalent in the dimer and monomer (N,N',S,S'), comparable values of formal redox potential ($E^{0\prime}$) can be assumed for both species. Consistent with this, in changing C_{Cu} (i.e., varying the dimer/monomer ratio), minimal shifts in the anodic (E_{PA}) and cathodic (E_{PC}) potentials can be detected for equivalent scan rates (ν). The only significant variation of ΔE_p with C_{Cu} is seen for $\mathbf{a_2}(BF_4)_2$ in CH_2Cl_2; in fact, at $\nu = 200$ mV s^{-1}, a difference of ΔE_p of 324 mV between the 0.01 and 0.001 M samples is detected (see Figure S17 of the Supporting Information).

An anomaly occurs for 0.001 M $\mathbf{b_2}(BF_4)_2$ in CH_2Cl_2, whose voltammograms present two cathodic (reverse) peaks (see Figure S17 of the Supporting Information): one corresponding to the diffuse peak found in other conditions (concentrations and solvent) and the second appearing at higher potentials. The intensity of the latter increases much faster with ν, so that it can be tentatively interpreted as an irreversible "pre-peak" originating from a strong adsorption of a Cu^{I} species on the electrode surface.[47] When C_{Cu} (0.01 M) is increased, the absorption becomes weaker with respect to diffusion and, therefore, is no longer detectable (see Figure S16 of the Supporting Information).

Conclusions

The scorpionate N,N',S,S'-donor ligands L^a and L^b were synthesized. The Cu^{I} complexes $[Cu(L^a)]_2](BF_4)_2$ ($\mathbf{a_2}(BF_4)_2$) and $[Cu(L^b)]_2](BF_4)_2$ ($\mathbf{b_2}(BF_4)_2$) are dinuclear at the solid state, with each copper center exhibiting a distorted tetrahedral N,N',S,S' coordination environment. However, the crystal structures of the complexes do not completely reflect the solution properties. In fact, in acetonitrile, there is evidence of mononuclear species in equilibrium with the dimers. In particular, the aggregation processes were quantitatively analyzed by means of ^1H NMR dilution titrations, which allowed for the determination of the thermodynamic parameters of the dimerization reactions: $\mathbf{2a}^+ = \mathbf{a_2}^{2+}$ and $\mathbf{2b}^+ = \mathbf{b_2}^{2+}$. The equilibrium constant (K^0) was measured in the 280–310 K range, yielding a negative ΔH^0 and, surprisingly, a positive ΔS^0. The latter suggests that dimerization may be entropy-driven because of a better solvation in the monomers with respect to the dimers, resulting in the release of solvent molecules in the association. Furthermore, ^1H PGSE NMR experiments performed at different C_{Cu} provided a weighted-average hydrodynamic volume (V_H) of the exchanging species. The combination of ^1H NMR titration with ^1H PGSE NMR data (log K^0 and V_H, respectively) allowed us to determine the hydrodynamic volumes of the individual species (V_H^0(M) and V_H^0(D)). The applied procedure is analogous to one that was recently reported and that combines PGSE and conductometric data.[49] As cyclic voltammetry attests, the complexes $\mathbf{a_2}(BF_4)_2$ and $\mathbf{b_2}(BF_4)_2$ show a quasi-reversible to irreversible behavior of the Cu^{I}/Cu^{II} redox couple (CH_3CN and CH_2Cl_2), with quite high ΔE_p values (in the 0.2–0.9 V range for $\mathbf{a_2}(BF_4)_2$ and in the 0.6–1.1 V range for $\mathbf{b_2}(BF_4)_2$). Presumably, this is due to the flexibility of the ligands, especially the alkyl-thioether groups, which confer to the complexes a considerable conformational freedom, implying a high reorganization energy involved in the electron transfer.

Acknowledgment. This work was supported by the Ministero dell'Istruzione, dell'Università e Ricerca (Rome, Italy).

Supporting Information Available: Crystallographic information files (CIF) for $\mathbf{a_2}(BF_4)_2 \cdot 2CH_2Cl_2$, $\mathbf{b_2}(BF_4)_2$, $[Cu(L^b)Cl_2]$, and $[Cu(L^a)_2(H_2O)](OTf)_2 \cdot H_2O \cdot CH_3OH$; Ortep molecular structures of $[Cu(L^b)Cl_2]$ and $[Cu(L^a)_2(H_2O)](OTf)_2 \cdot H_2O \cdot CH_3OH$; Cartesian coordinates of the optimized structures (B3LYP/lanl2dz) of $\mathbf{a}^+$ and $\mathbf{b}^+$; stacking plots of the ^1H NMR spectra of $\mathbf{a_2}(BF_4)_2$ and $\mathbf{b_2}(BPh_4)_2$ in CD_3CN; distribution diagrams of $\mathbf{a_2}(BF_4)_2$ and $\mathbf{b_2}(BF_4)_2$ in CD_3CN at different temperatures; van't Hoff plots for the dimerization equilibria; mathematical derivation of eq 1; and cyclic voltammetry of $\mathbf{b_2}(BF_4)_2$. This material is available free of charge via the Internet at http://www.pubs.acs.org.

IC702108X

(49) Ciancaleoni, G.; Zuccaccia, C.; Zuccaccia, D.; Macchioni, A. *Organometallics* **2007**, *26*, 3624–3626.